Evolution of Alfvénic Wave Packets to Turbulence and Chaos in Plasmas

B. Buti

Jet Propulsion Laboratory,

California Institute of Technology,

Pasadena, CA 91109

Spatio-temporal evolution, of large-amplitude Alfvén waves, is investigated by means of their characteristic evolution equations as well as by MHD simulations. Conditions for the occurence of phenomena of self-organization, collapse and disruption of solitons are derived. Evolution of coherent Alfvén waves, driven by a harmonic driver, into chaos and turbulence is presented. Similarities and differences, of the two approaches used, are pointed out. This article is essentially an overview of the turbulent and chaotic Alfvén waves.

I. INTRODUCTION

Alfvén waves are a ubiquitous feature of magnetoplasmas. Implications of existence of large-amplitude Alfvén waves in many cosmic plasmas have been investigated. Some of these examples include turbulent heating of solar corona[1], coherent radio emissions[2], interstellar scintillations of radio sources[3], generation of stellar winds and extragalactic jets etc.[4] Alfvén wave trains as well as Alfvénic turbulence have long been observed in the solar wind[5,6]. Recently Burlaga[7] reported observations of some chaotic features , like multifractals and intermittent turbulence in the solar wind. Observations of Alfvénic intermittent turbulence are also reported by Marsch and Liu[8] and Tu and Marsch[9]. From the Helios spacecraft data for the slow - speed solar wind flow, Macek[10] has concluded the presence of an attractor. All these observations are clear indications of the significance of investigating the nonlinear and chaotic behaviour of Alfvén waves. In the present paper, we have tried to give an overview of the chaotic and turbulent Alfvén waves.

To study the dynamical behaviour of large-amplitude Alfvén waves, one can either use the full set of dispersive MHD equations and be satisfied with their numerical solutions or use an evolution equation derived from these MHD equations. The most popular evolution equation, governing nonlinear Alfvén waves, is the Derivative Nonlinear Schrödinger (DNLS) equation[11–14]. The big advantage of dealing with the DNLS is that it can be solved analytically[11,15,16]. Kaup and Newell[11] had obtained its solution by means of Inverse Scattering Transform (IST) method. They also showed that any evolution equation, e.g., the DNLS would give a soliton solution independent of the initial condition used to solve the evolution equation. However, one should bear in mind that the DNLS is derived on the assumption that plasma β (ratio of the kinetic pressure to the magnetic pressure) is not ~ 1. For systems with $\beta \sim 1$, kinetic effects[14,17–19] as well as coupling between magnetic field flutuations and density fluctuations[20] become significant. To incorporate these effects in the studies of nonlinear dynamical Alfvén waves, one has to do MHD[21,22] and kinetic

simulations[23]. These simulations show that the Alfvén solitons get disrupted. Moreover, we see the steepening of these waves besides the emission of radiation. On the other hand, the driven DNLS equation leads to chaos and turbulence in the Alfvénic systems [24–28].

II. EVOLUTION EQUATIONS FOR NONLINEAR ALFVÉN WAVES

The governing equations for large-amplitude Alfvén Waves in a dispersive medium, like a magneto-plasma, are the dispersive MHD equations:

$$\frac{\partial \rho}{\partial t} + \nabla \cdot (\rho \mathbf{v}) = 0, \tag{1a}$$

$$\rho \frac{d\mathbf{v}}{dt} = -\nabla p + \mathbf{J} \times \mathbf{B}, \tag{1b}$$

and

$$\frac{\partial \mathbf{B}}{\partial t} = \nabla \times \left[(\mathbf{v} \times \mathbf{B}) - \frac{1}{\rho} (\nabla \times \mathbf{B}) \times \mathbf{B} \right]. \tag{1c}$$

In eq.(1), $\mathbf{B}$ is normalized to B_0, ρ to ρ_0, $\mathbf{v}$ to $V_A = B_0/(4\pi\rho_0)^{1/2}$ (V_A being the speed of Alfvén Waves), t to inverse of Ω_i, the ion cyclotron frequency and l to V_A/Ω_i. The subscript '0' refers to the equilibrium quantities. Note that the second term on the right hand side of Eq.(1c) is due to ion inertial effects in the generalized Ohms law. We may point out that the set of Eqs.(1) holds good for multi-species plasmas[16] with appropriately defined mass density ρ and pressure p. However, in this section we will consider only two-species plasmas.

A. Derivative Nonlinear Schrödinger Equation

We would like to point out here that the set of equations (1) would not be valid for systems with β of order of unity because in that case the kinetic effects become important. Moreover

for $\beta \sim 1$, coupling between Alfvén waves and ion acoustic waves becomes significant[20,29] . For wave propagation along the direction of a uniform magnetic field i.e., along x - axis, Eqs.(1) simplify to :

$$\frac{\partial \rho}{\partial t} + \frac{\partial}{\partial x}(\rho v_x) = 0, \tag{2}$$

$$\frac{\partial}{\partial t}(\rho v_x) + \frac{\partial}{\partial x}(\rho {v_x}^2) + \frac{\partial \beta}{\partial x} + \frac{\partial}{\partial x}\left(\frac{B^2}{2}\right) = 0, \tag{3}$$

$$\frac{\partial}{\partial t}(\rho \tilde{v}) + \frac{\partial}{\partial x}(\rho v_x \tilde{v}) - \frac{\partial B}{\partial x} = 0, \tag{4}$$

$$\frac{\partial B}{\partial t} + \frac{\partial}{\partial x}(v_x B - \tilde{v}) = -i\frac{\partial}{\partial x}\left(\frac{1}{\rho}\frac{\partial B}{\partial x}\right), \tag{5}$$

and

$$\frac{\partial \beta}{\partial t} + \frac{\partial}{\partial x}(\beta v_x) + (\gamma - 1)\beta \frac{\partial v_x}{\partial x} = 0, \tag{6}$$

where v_x is the flow velocity along the direction of propagation, γ is the ratio of the specific heat, $B = (B_y + i\, B_z)$ and $\tilde{v} = (v_y + i\, v_z)$. For pressure, we have used the adiabatic equation of state i.e., $p\rho^{-\gamma} = const.$

For $\beta \neq 1$, these equations have been simplified by using reductive perturbation methods[16,30–32]. For magnetic fluctuations carried to third order, they yield the following evolution equation:

$$\frac{\partial B}{\partial t} + \frac{1}{4\,(1-\beta)}\frac{\partial}{\partial x}\left(B \mid B \mid^2\right) \pm \frac{i}{2}\frac{\partial^2 B}{\partial x^2} = 0. \tag{7}$$

Equation (7) is the well known derivative nonlinear Schrödinger (DNLS) equation. The plus and minus signs in the last term correspond to left and right hand polarization respectively. Equation (7) can be solved analytically; its exact solution is given by[11,16]:

$$B\,(x,\, t) \;=\; \frac{(2^{1/2} - 1)^{1/2}\; B_s\; e^{i\theta\,(x)}}{[2^{1/2}\;\cosh\,(2\;V_s\;x)\;-\;1]^{1/2}}, \tag{8}$$

where B_s is the amplitude of the soliton,

$$\theta\,(x,t) \;=\; -\,V_s\,x \;+\; 3\,\tan^{-1}\,[(2^{1/2}+1)\,\tanh(2V_s\,x)]. \tag{9}$$

θ is the phase and V_s is the soliton speed defined by,

$$V_s \;=\; \frac{(2^{1/2}-1)\,B_s^2}{8\,(1\;-\;\beta)}. \tag{10}$$

Hada et al.[15] had shown that Eq.(7) can give a variety of solutions, namely, (1) periodic envelope modulations; (2) monochromatic waves; (3) hyperbolic solitons; (4) algebraic solitons. On using the Lagrangian approach, Kennel et al.[12] had derived the vector derivative nonlinear Schrödinger (VDNLS) equation that governs elliptically polarized Alfvén Waves.

B. Modified Derivative Nonlinear Schrödinger Equation

The DNLS / VDNLS equations discussed in the previous subsection are strictly valid for plasmas with homogeneous densities and magnetic fields. By using the reductive perturbation method, Buti[33] had rederived the governing evolution equation for Alfvén waves in inhomogeneous plasmas. In this derivation, even though no explicit assumption about the homogeneity of the magnetic field was made, implicitly the field considered was homogeneous because of the slab geometry used. To overcome the restrictions imposed by this implicit assumption, Buti et al.[34] have incorporated spherical geometry. On using equations (1) in spherical co-ordinates and assuming no variations along θ and ϕ directions i.e., $\partial/\partial\theta = \partial/\partial\phi = 0$, Eqs. (1) reduce to:

$$\frac{\partial\rho}{\partial t} + \frac{1}{r^2}\frac{\partial}{\partial r}(r^2\rho v_r) = 0, \tag{11a}$$

$$\rho\frac{dv_r}{dt} = -\frac{\partial p}{\partial r} - \frac{\partial}{\partial r}\frac{B_\perp^2}{2} - \frac{B_\perp^2}{2}, \tag{11b}$$

$$\rho\frac{d\mathbf{v}_\perp}{dt} = \frac{B_r}{r}\frac{\partial}{\partial r}(r\mathbf{B}_\perp), \tag{11c}$$

and

$$\frac{\partial \mathbf{B}_\perp}{\partial t} = \frac{1}{r}\frac{\partial}{\partial r}(B_r v_\perp - v_r B_\perp) + \frac{1}{r}\frac{\partial}{\partial r}\left[\frac{B\hat{\mathbf{e}}_r}{r\rho} \times \frac{\partial(\mathbf{B}_\perp r)}{\partial r}\right], \tag{11d}$$

where r is the radial distance, $\mathbf{B}_\perp = (B_\theta, B_\phi), \mathbf{v}_\perp = (v_\theta, v_\phi)$, and $B_\perp^2 = (B_\theta^2 + B_\phi^2)$. Once again, for pressure, we use the adiabatic equation of state i.e., $p\rho^{-\gamma} = const.$ In order to satisfy eq.(8a) and the condition, $div\ \mathbf{B}_0 = 0$, the equilibrium density $\rho_0(r)$ and the magnetic field $B_0(r)$ must satisfy the conditions:

$$B_0(r)\, r^2 \;=\; const \tag{12}$$

and

$$\rho_0(r)\, U(r)\, r^2 \;=\; const. \tag{13}$$

For weakly nonlinear systems, we can use reductive perturbation scheme to derive the evolution equation from Eqs.(11). Following the procedure outlined in Buti[33], we use the following stretchings:

$$\eta = \epsilon^2 r; \qquad \xi = \epsilon\left[\int \frac{dr}{V(r)} - t\right]. \tag{14}$$

In Eq.(11) ϵ is the stretching parameter and $V(r)$ is the phase velocity of the Alfvén wave that is given by

$$V(r) = U(r) + \frac{B_0(r)}{\rho_0^{1/2}(r)}. \tag{15}$$

In Eq.(15), U is the equilibrium streaming plasma velocity.

On using the expansions for density, velocity, pressure and magnetic field appropriate to Alfvén Waves (cf. Buti[33]), for a spherically symmetric system, we obtain the following

evolution (MDNLS) equation:

$$\frac{\partial B}{\partial \eta} + \frac{3\,U}{2\,V\,\eta}\,B + \frac{B}{4\,V\,(V-U)}\,\frac{\partial}{\partial \eta}\left(V^2 - U^2\right) + \frac{(V-U)}{4\,B_0^2(\eta)\,V^2\,(1-\beta(\eta))}\,\frac{\partial}{\partial \xi}\left(B \mid B \mid^2\right) + \frac{i\,(V-U)^2}{2\,V^3\,B_0(\eta)}\,\frac{\partial^2 B}{\partial \xi^2} = 0, \tag{16}$$

where $B = (B_\theta + i\,B_\phi)$, $\beta(\eta)$ is the plasma β, and $B_0(\eta)$ is the ambient magnetic field. In deriving Eq. (16), we have taken wave propagation as well as the ambient magnetic field along the radial direction. As in the case of the DNLS, here also we have neglected fifth order nonlinear terms. This equation, however, is valid for arbitrary inhomogeneities. We may note that for nonstreaming uniform plasmas i.e., for $U = 0$ and $\rho_0(r) = 1$, $V \to 1$ and Eq. (16) reduces to Eq.(7). It is worth noting that the roles of spatial and temporal variables are interchanged. It is interesting to observe that this modified DNLS (Eq (16)), besides having additional two linear terms in B, has variable co-efficients for nonlinear and dispersive terms. Because of these complicated variable co-efficients, it is not possible to find an analytical solution to Eq. (16) and one has to look for its numerical solution.

Equation (16) has been solved numerically by means of the spectral collocation method. For the sake of computational convenience, we rewrite this equation as,

$$\frac{\partial B}{\partial \eta} + f(\eta)B + \alpha_1(\eta)\frac{\partial}{\partial \xi}(|B|^2 B) + i\alpha_2(\eta)\frac{\partial^2 B}{\partial \xi^2} = 0. \tag{17}$$

Since eq. (17) has temporal and spatial variables interchanged, we write the approximate solution for B as a Fourier expansion in time instead of space, namely

$$B(\xi, \eta) = \sum_{k=-N}^{N-1} b_k(\eta) e^{-i\lambda_k \xi}. \tag{18}$$

Note that B is assumed to be periodic in time, with period T and frequency $\lambda_k = 2\pi k/T$. For evaluation of the cubic nonlinear term of eq.(17), we use the 3/2 rule for dealiasing[35].

According to this scheme, the Fourier transform for the nonlinear term can be represented by,

$$|B(\xi_i,\eta)|^2 B(\xi_i,\eta) = \sum_{k=-M}^{M-1} g_k(\eta) e^{-i\lambda_k \xi_i}. \tag{19}$$

In order to be sure that aliasing errors are not introduced by this form of approximate solution, summation index M must be greater than $3N/2$; N is the summation index used in Eq.(18). This simply means that the nonlinear term is calculated by using larger number of grid points compared to the number used in the original expansion for B in Eq. (18).

For the numerical solution of the MDNLS, we do not need to introduce any artificial dissipation . In our case, inhomogeneous terms formally play the role of effective dissipation. Moreover, the iterative scheme of dealiasing, that we have used for calculating nonlinearity, keeps the soliton solution of the conservative homogeneous DNLS unchanged for much longer distances than reported here. This could alternatively be achieved even without dealiasing, but with a much finer grid. As mentioned earlier, the problem of wave propagation is solved as an evolutionary problem in space. For this purpose, we assume that there is an influx of waves at one end of the interval (e.g., closer to the Sun in case of the solar wind plasma) and the waves are propagating outward. The influx is assumed periodic in time.

For the numerical solution, we have considered the evolution of an initial Alfvén soliton which is an exact solution of the DNLS equation and is given,

$$B\,(\xi,\ r_0)\ =\ \frac{B_{max}\ e^{i\theta\,(\xi)}}{cosh^{1/2}\psi}, \tag{20}$$

with

$$\psi\ =\ (\xi\ -\ L/2)\ B_{max}^2\ /(\ 2\ \delta), \tag{21}$$

$$\theta\,(\xi)\ =\ \frac{3}{2}\ tan^{-1}\,(sinh\ \psi) \tag{22}$$

and

$$\delta = \frac{2}{V}(1 - \beta)(V - U). \tag{23}$$

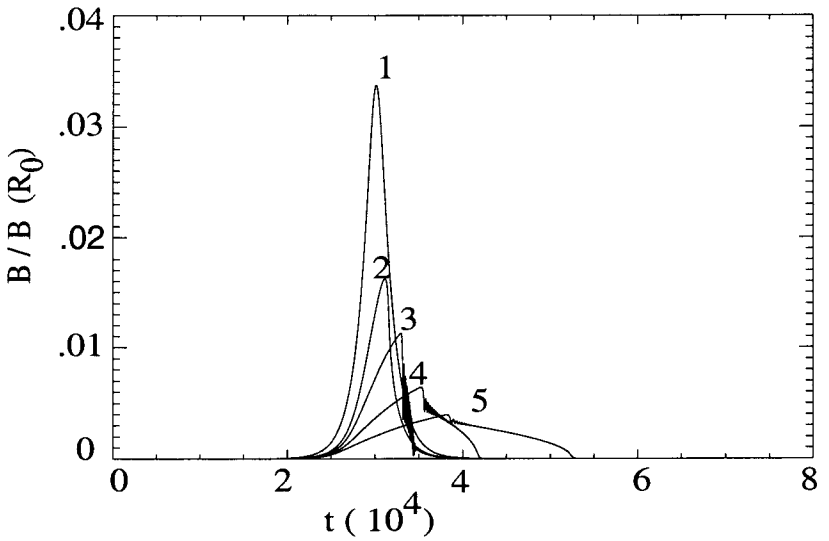

FIG. 1. Shows the evolution of B / $B_0(r_0)$ with t for B_{max} (R_0) = 0.036, R_0 = 0.1 AU, U_0 = 1.5 V_{A0} and β (R_0) = 0.05. Curves labelled 1, 2, 3, 4 and 5 correspond to r = 0.1 AU, 0.35 AU, 0.5 AU, 0.7 AU and 0.9 AU.

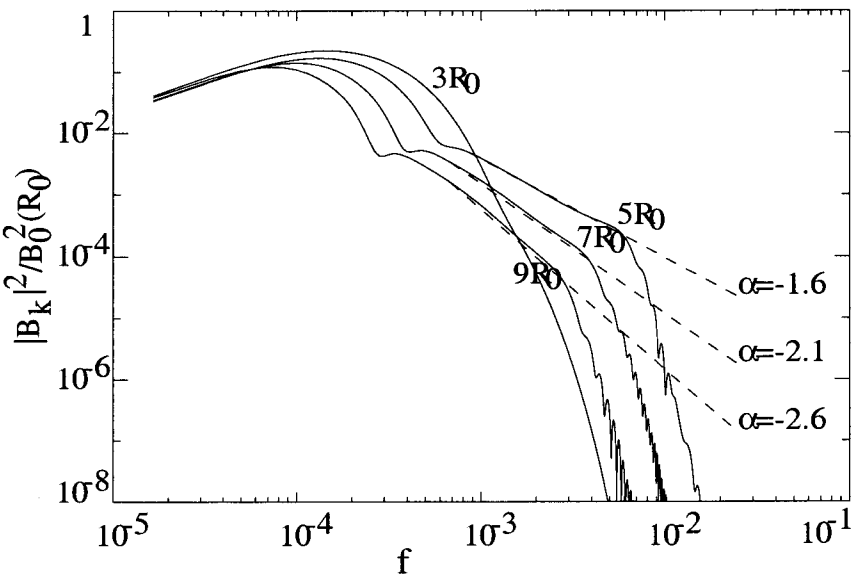

FIG. 2. Shows the power spectra for magnetic field at heliospheric distances 0.3 AU, 0.5 AU, 0.7 AU and 0.9 AU. The parameters used are same as for Fig.1.

B_{max} in Eq.(20) is the amplitude of the initial soliton normalized to B_0 (r_0) and L is the

simulation box length. We would like to point out that the solution given in Eq.(20) is different than the one given by Eq.(8). In the soliton solution[36] of the DNLS equation, there are two arbitrary constants κ_0 and ν_0. For Eq.(8), we had taken $\nu_0 = 0$ and now for Eq.(20) κ_0 has been taken to be zero.

The time evolution of the DNLS soliton at different spatial distances, from the reference point r_0, is shown in Fig.1. For the case of Alfvén waves propagating away from the sun in the interplanetary medium, this reference point could be $R_0 = 0.1AU$. From this figure, we clearly see the dissipative effects of the inhomogeneities. The amplitude of the soliton goes down as it propagates. Similar dissipative effects of inhomogeneities, in connection with modulated ion-acoustic waves, were reported by Mohan and Buti[37]. We also see the steepening of the wave and the high-frequency radiation on the leading edges. MHD simulations (see sec.5) aso show similar behaviour. The frequency spectra for the magnetic field intensites are shown in Fig.2. The spectral index, for the power-law spectra, is increasing with the heliocentric distance. We also see breaks in the spectra. The break-point moves to the lower frequencies with the increasing distances from the sun. Similar features have been observed in the turbulent solar wind spectra[5,38] by Mariner 5 and Helios 1 and 2. Buti et al.[34] had looked into the evolution of initial circulatly polarized Alfvén waves. The evolution in this case was found to be much slower compared to the case of the DNLS soliton.

III. DRIVEN ALFVÉN WAVES

In section II. we have shown that the finite amplitude Alfvén waves, in a homogeneous plasma, are governed by the DNLS equation that gives coherent structures like solitons. However if there is any dissipation/damping in the system, one finds shocks instead of solitons[39]. In this section, we will present the dynamics of nonlinear driven Alfvén waves. For the present discussion, we have picked up a simple harmonic driver, which modifies the

DNLS equation to

$$\frac{\partial B}{\partial t} + \frac{1}{4\,(1-\beta)}\frac{\partial}{\partial x}\left(B \mid B \mid^2\right) \pm \frac{i}{2}\frac{\partial^2 B}{\partial x^2} = a\; e^{i(\kappa x - \Omega t)}, \tag{24}$$

where a is the amplitude of the driver. The external driver in Eq.(24) simply acts as a source, which kills the coherent properties of the solitons. In case of localized stationary Alfvén waves, it has been shown[13,31,32,39] that Eq.(24) leads to chaos under certain conditions. Unlike the DNLS Eq.(7), Eq.(24) can not be solved analytically. This equation is solved by spectral-collocation method with periodic boundary conditions. For the initial condition we take a solitary Alfvén wave packet, namely

$$B\,(x,\; t=0) \;=\; \frac{(2^{1/2}-1)^{1/2}\; B_s\; e^{i\theta\,(x)}}{[2^{1/2}\;\cosh\,(2\;V_s\;x)\;-\;1]^{1/2}}, \tag{25}$$

where B_s is the amplitude of the soliton,

$$\theta\,(x, t=0) = -V_s x + 3\tan^{-1}[(2^{1/2}+1)\tanh(2V_s x)] \tag{26}$$

and V_s is the soliton speed defined by,

$$V_s \;=\; \frac{(2^{1/2}-1)\;B_s^2}{8\;(1\;-\;\beta)}. \tag{27}$$

Note that Eq. (25) is the super-Alfvénic soliton solution of Eq.(7) in the wave frame of reference[16]. Earlier, Nocera and Buti[27] had looked into the evolution of the driven algebraic solitons of Eq.(7) and had found that they decay into hyperbolic solitons.

A. Chaotic Alfvén waves

The modulational instability of the DNLS Eq.(7) is known to depend on the sign of the product of the co-efficients of the nonlinear and the dispersive terms. Cosequently for $\beta < 1$, right-hand polarized (RHP) soliton is supposed to be more stable compared to the left-hand polarized (LHP) soliton. For $\beta > 1$, the stability properties are reversed. Our numerical simulations of Eq.(24) also confirm these conclusions. Unlike fusion plasmas, solar wind

has a variable β, which, depending on the distance from the sun, can be < 1 or even > 1. Closer to the sun, where Alfvén Waves are supposed to be generated, $\beta < 1$ and hence RHP driven soliton should be more robust. This is indeed the case (cf. Fig.4). We observe that the LHP soliton very quickly, even for a relatively weak driver, loses its coherent properties and goes into a chaotic state. For numerical calculations, we have scaled Eq.(24) and have taken $L = 800$ (L is the simulation box length), $\beta = 0.1$, $\kappa = 0.08, \Omega = 10^{-4}$ and $B_s = 0.5$. The values of κ and Ω used here are arbitrary. We could pick up different numbers but the resultant qualitative behaviour does not change. This driver could be easily taken as another coexisting wave; for this κ and Ω would be related through its dispersion relation. Our exercise here is a first step to be followed by a different variety of drivers e.g., a pulse, a beam etc. For the parameters used for the present calculations, the speed of the initial soliton, in the solar wind frame of reference, turns out to be $1.025V_A$. The super-Alfvénic nature of the soliton is simply because we have used the super-Alfvénic solution (25) for the DNLS Eq.(7). The corresponding width of the soliton, which is given by $1/(2V_S)$, is ~ 20 ion inertial lengths. We believe that such large amplitude pulses, distributed over very many ion inertial lengths, have been observed in space plasmas.

Fig.3 shows the time evolution of the driven left-hand soliton for various amplitudes of the harmonic driver. We find that even for an extremely weak driver with amplitude $A = 0.003$, LHP wave becomes chaotic at $\tau \sim 5 \times 10^5$ (cf. Fig 3a). Note that $\tau = t/(144)$ and A is the scaled amplitude ; $A = (12^{3/2})a$. The time-series corresponding to somewhat stronger drivers namely, A = 0.03 and 0.1 are shown in Figs.3b and 3c. From these two figures, we see that the chaos sets in at $\tau \sim 5 \times 10^4$ and at $\tau \sim 1.48 \times 10^4$ for $A = 0.03$ and $A = 0.1$ respectively. It is interesting to note that the time at which Alfvénic system becomes chaotic scales as A^{-1}.

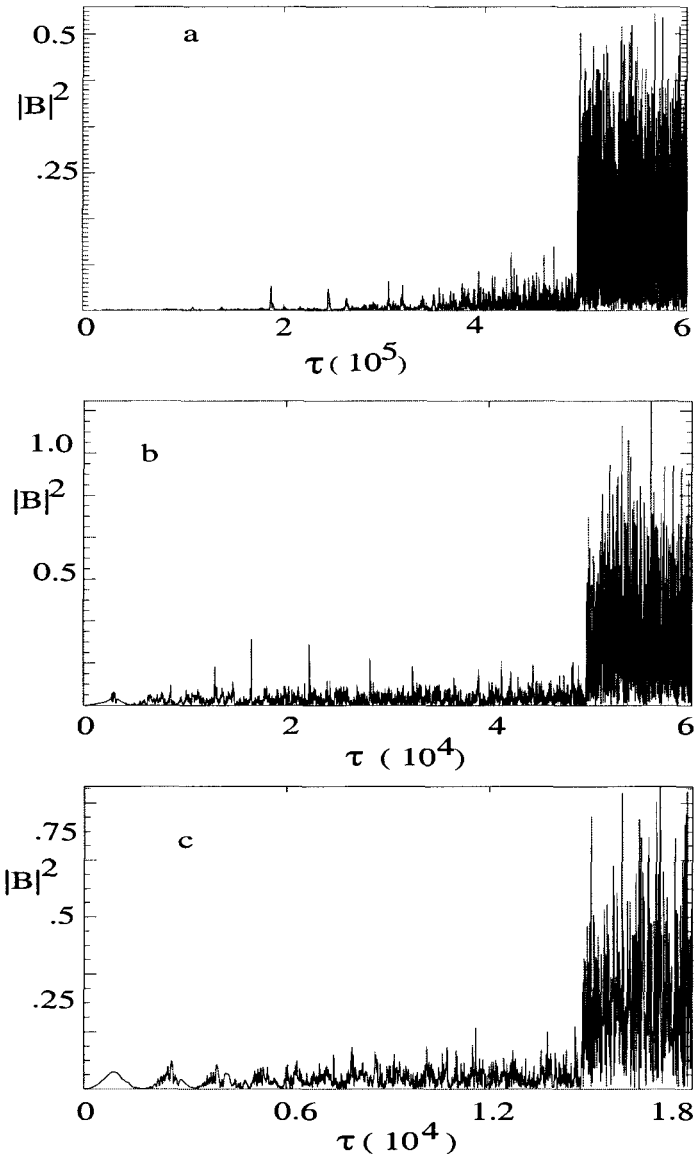

FIG. 3. Transition of left-hand polarized soliton to chaos a) at $\tau \sim 5 \times 10^5$ for $A = 0.003$, b) at $\tau \sim 5 \times 10^4$ for $A = 0.03$, c) at $\tau \sim 1.48 \times 10^4$. for $A = 0.1$. Note that $\tau = t/144$.

In contrast, the RHP soliton is found to be much more robust as expected from the DNLS equation. Time evolution, of RHP soliton at $x = L/8$ (L being the length of the simulation box),is shown in Fig.4 for $A = 0.01$ (Fig.4a), 0.1 (Fig.4b) and 0.5 (Fig.4c). Unlike the case of LHP soliton, RHP goes into a chaotic state only when it is driven by a real strong driver with $A = 0.5$. In case of weaker drivers (cf. Fig.4a, 4b), only low level turbulence is generated which is seen in between the perturbed solitons. For this weak turbulence we have calculated the space as well as time correlations and we find that the time correlations

are destroyed much more quickly compared to the space correlations[40].

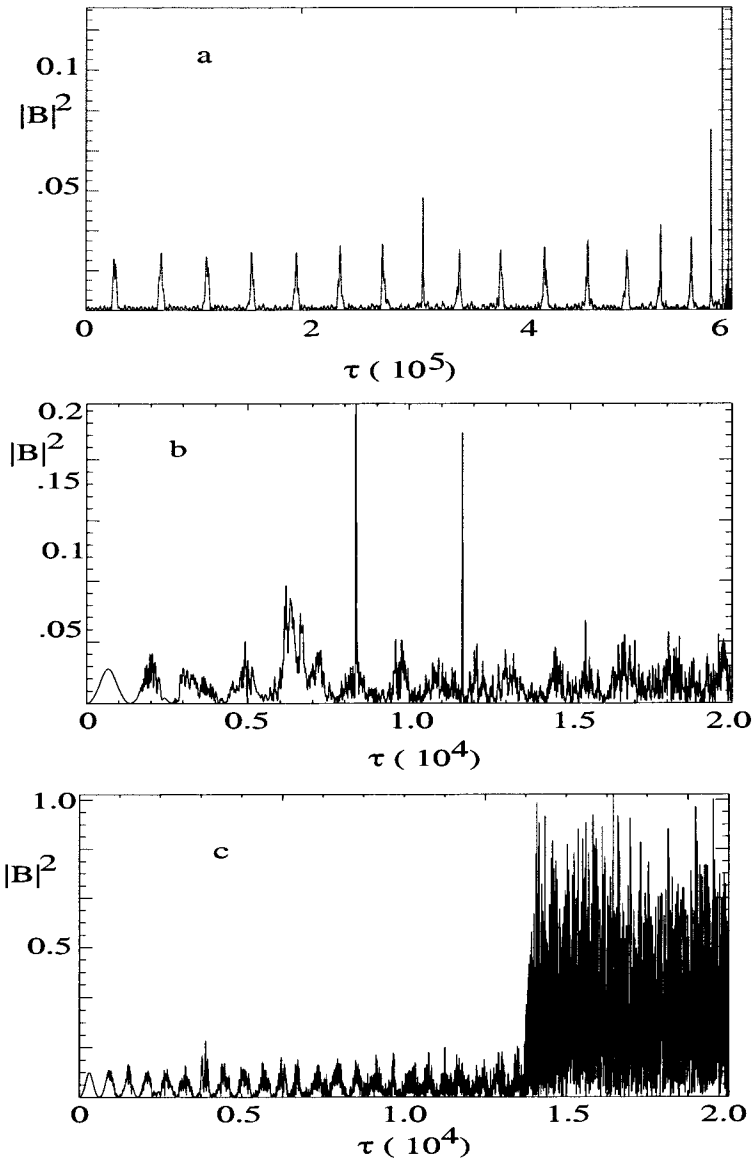

FIG. 4. Time series for evolution of RHP soliton at $x = L/8$ for a) $A = 0.01$, b) $A = 0.1$, c) $A = 0.5$.

To get an insight into the spectral behaviour of RHP Alfvén solitons, we have done high-resolution investigations of the time series. This is presented in Fig.5. This figure illustrates the time evolution of the turbulence shown in Fig.4a after a jump in the phase of the driver $\Delta\Phi = 2.876$ was imparted at $\tau = 5.3 \times 10^5$.

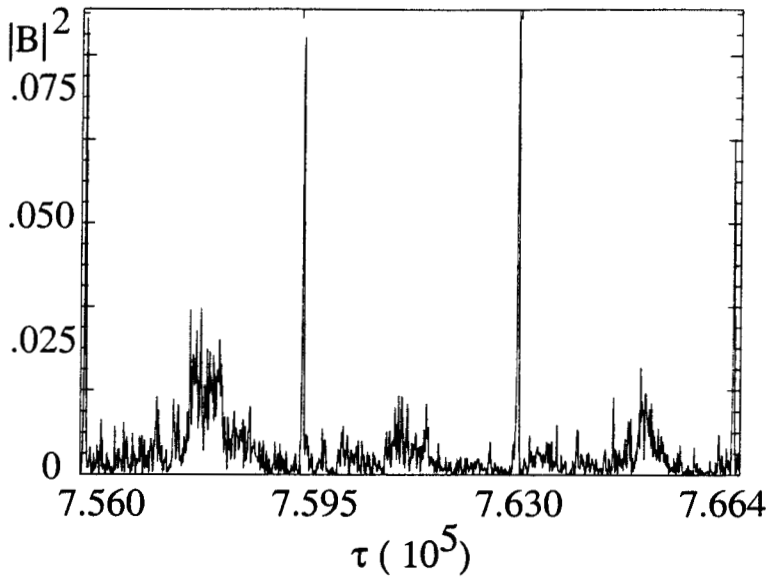

FIG. 5. Time evolution of the turbulence shown in Fig.4a during $7.56 \times 10^5 < \tau < 7.66 \times 10^5$.

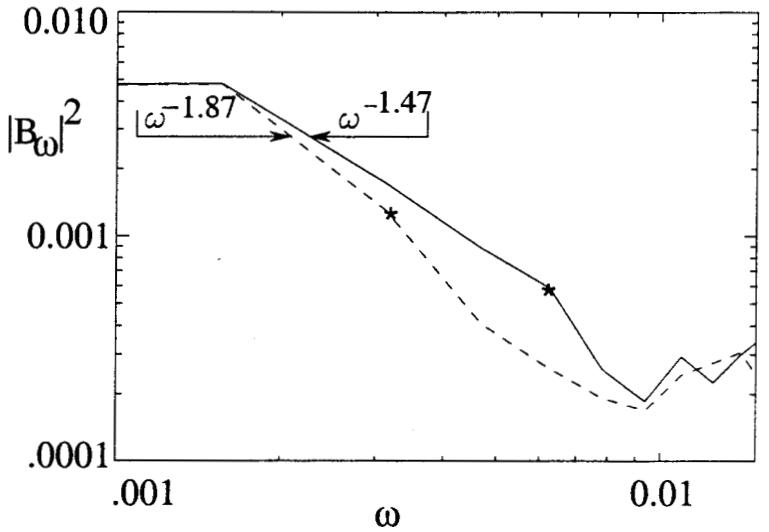

FIG. 6. Evolution of frequency spectral index from 1.47 for the turbulence (shown in Fig.5) in the interval $7.595 \times 10^5 < \tau < 7.630 \times 10^5$ (solid line) to 1.87 for turbulence during $7.630 \times 10^5 < \tau < 7.665 \times 10^5$ (dotted line).

The frequency spectra for the turbulence in two intervals, namely, $7.595 \times 10^5 < \tau < 7.630 \times 10^5$ (solid line) and $7.630 \times 10^5 < \tau < 7.665 \times 10^5$ (dotted line) of Fig.5, are shown in Fig.6. The latter one shows two distinct features. First the frequency spectral index goes up from 1.47 to 1.87 with the propagation of solitons. Second we observe break-point (shown

by *) in the spectra. The break-point is found to move towards lower frequency with an increase in the spectral index. Similar trend has been reported in the observed solar-wind turbulence[38].

B. Self - Organization / Pattern Formation

Let us go back to the RHP soliton and drive it with a harmonic driver with amplitude $A = 0.01$. Its evolution at $\tau \sim 6 \times 10^5$ is shown in Fig.7a where we see a highly peaked soliton with $|B_{max}|^2 \sim 0.2$ coexisting with a very weak background turbulence. The width of this soliton, which is given by $(2\ V_S)^{-1}$, turns out to be approximately $1.7 R_g$ (R_g being the gyro-radius). Thus we are observing the 'collapsed' soliton. For the parameters used in section 3, R_g in our dimensionless units (V_A/Ω_i) is 0.4. Similar collapsed soliton for the case of the driver with $A = 0.1$ appears much earlier at $\tau \sim 1.4 \times 10^4$ and with much larger amplitude $|B_{max}|^2 \sim 0.5$ (shown in Fig.7b). The DNLS soliton, in our case is collapsing mainly due to its interaction with the driver. This is an altogether different process compared to the collapse of an NLS soliton which occurs because of multi- dimensional aspects[41] . We must bear in mind that while dealing with systems involving such small scale lengths, kinetic effects should be properly included.

In order to ascertain the cause of the collapse of the DNLS soliton, we introduced a jump $\Delta\Phi = 2.876$ in the phase $\Phi = (\kappa x - \Omega t)$ of the driver at $\tau = 5.3 \times 10^5$ and then integrated Eq.(24) to determine its evolution between $\tau = 5.3 \times 10^5$ and $\tau = 8 \times 10^5$. The resulting evolution at $\tau = 8 \times 10^5$ is shown in Fig.8. Once again we see the bifurcation of the solution from one peak of Fig.7 to four peaks of Fig.8. Here we find a much bigger surprise. The four narrow pulses in Fig.8 turn out to be the four solitons of our original nondriven DNLS equation (7). This is a clear demonstration of Self-Organization phenomena. The energy stored in the original one soliton, because of its interaction with the driver, is redistributed

into the final four solitons which have speeds four times that of the original soliton i.e., 4 V_s.

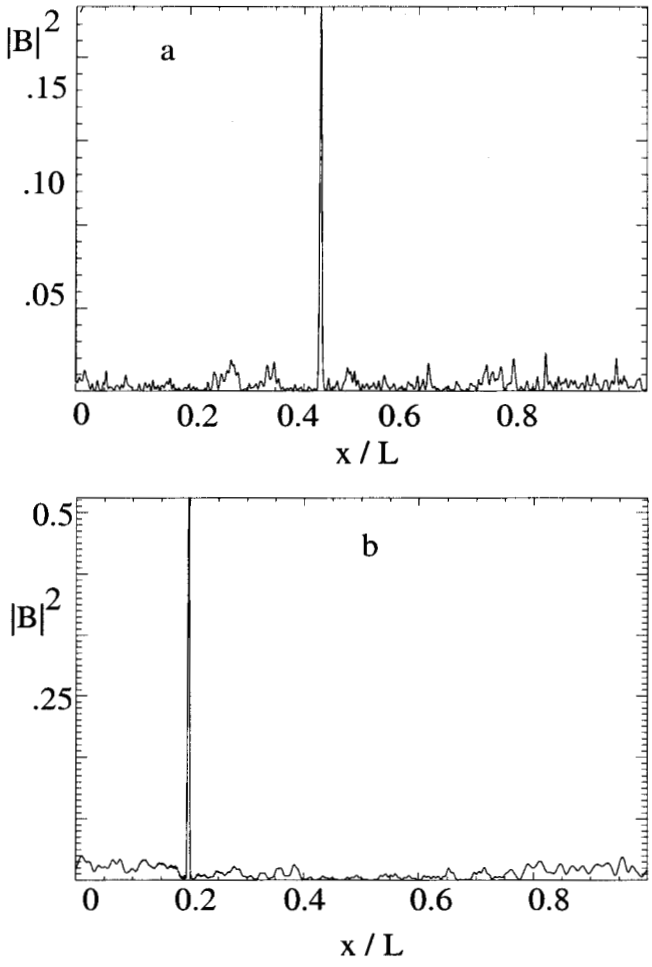

FIG. 7. Collapse of RHP soliton due to the driver with a) $A = 0.01$ at $\tau \sim 6 \times 10^5$ and b) $A = 0.1$ at $\tau \sim 1.4 \times 10^4$.

In order to determine whether the self-organization / pattern formation are characteristics of the initial soliton condition or of the evolution equation itself i.e., the DNLS, we had repeated our calculations for an initially structureless DNLS equation. Once again we found that the right-hand solutions are stable and appear as elliptic oscillations[27,42]. The left-hand solutions, on the other hand, do start with elliptic solutions but unlike RHP solutions they are found to be unstable. These ellipitic solutions in turn bifurcate into the bell-shaped wave packets. The latter (bell-shaped) solution is also not stable. The elliptic and the bell-shaped solutions appear alternatively[42]. So, we conclude that the self-organization is generic to the

DNLS equation.

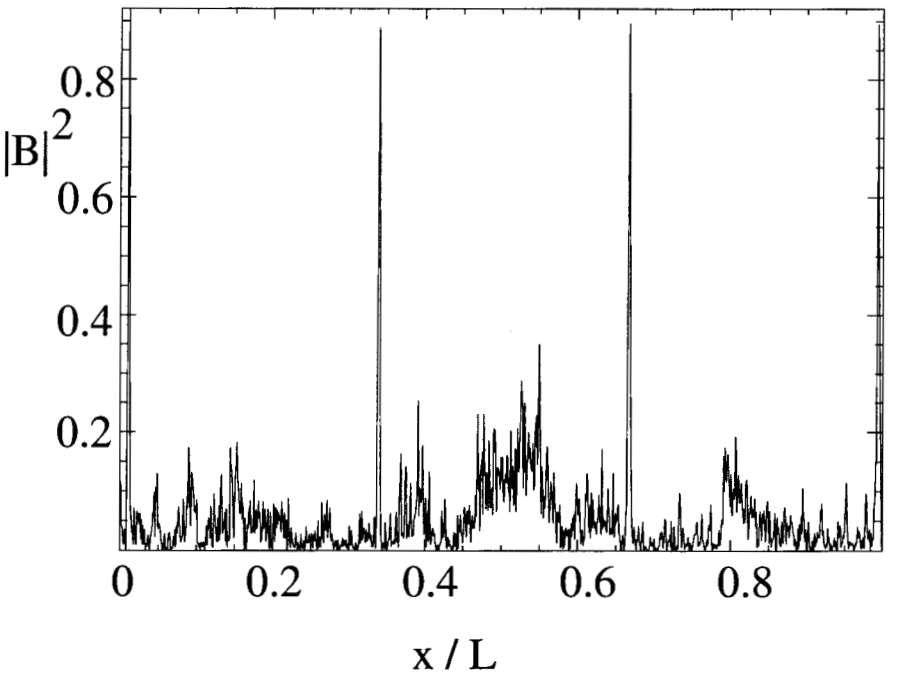

FIG. 8. Shows redistribution of energy into four solitons at $\tau \sim 8 \times 10^5$ due to a phase shift of 2.678 imparted to the driver at $\tau \sim 5.3 \times 10^5$.

C. Turbulence through Chaotic Channel

For the chaotic states shown in Figs. 3a-3c and in Fig.4c, we have calculated the power spectra for the magnetic field fluctuations. The results are shown in Fig.9. For LHP, with a very weak driving source ($A = 0.003$), we find an exponentially decaying energy spectrum. On the other hand, for the chaotic states shown in Fig.3c and Fig.4c, the magnetic energy scales as k^{-1} and for the case of chaos shown in Fig.3b, it scales as $k^{-1.5}$. These indeed are the features of a fully developed turbulence. In all the three cases we do see a break in the spectral index. These results have a lot of resemblance with the observations of solar-wind turbulence reported by Bavassano et al.[38]. These results are in contrast to the general feeling that the turbulence can be generated only by an infinite (or a very large) number of modes. However one can view the scenario presented here as analogous to the system with a finite but large number of modes. This is indicated by Figs.9a-9c, which show that the energy is

distributed into a few tens of modes. It is worth noting that the turbulent spectra, presented in Fig.9, are simply due to chaos in the Alfvénic systems.

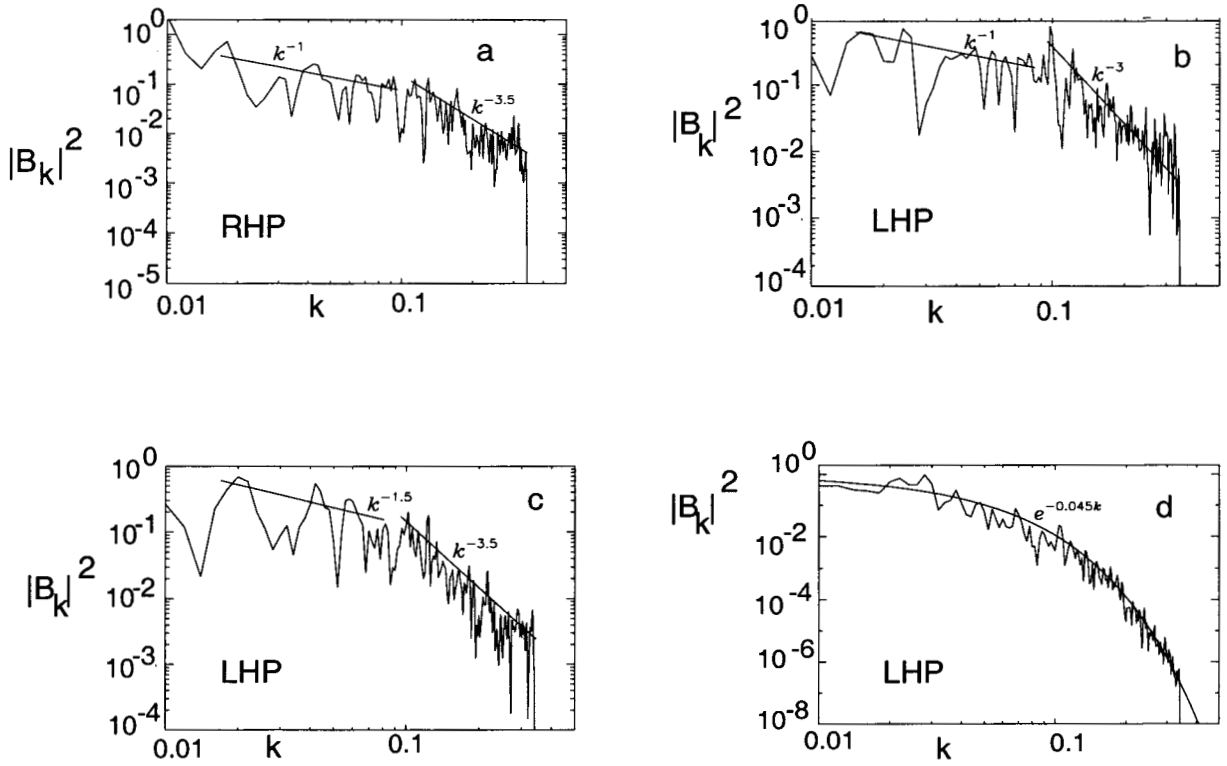

FIG. 9. Shows Spectra for magnetic field turbulence generated through chaos for a) RHP with $A = 0.5$, b) LHP with $A = 0.1$, c) LHP with $A = .03$ and d) LHP with $A = .003$.

IV. CONTROLLING CHAOS IN ALFVÉNIC SYSTEMS

The question of controlling chaos, in disssipative systems, was first discussed by Ott et al.[43]. The chaotic attractors, associated with dissipative dynamical systems, usually have a dense set of unstable periodic orbits embedded in them. Ott et al. suggested that one should first determine some of the low-period unstable periodic orbits embedded in the chaotic attractor. Then choose one, out of these unstable orbits, which yields improved performance when a small change is made in a parameter. Finally adjust the small parameter in such a way that the unstable periodic orbit is stabilized. Here we suggest an alternative way of controlling chaos in nondissipative systems e.g., a plasma which can be described as a driven

Hamiltonian system. As a specific example, we have chosen magnetoplasma with more than two species.

So far our discussion has been confined to plasmas with only two species e.g., hydrogen plasma. Very often, we encounter multispecies plasmas with electrons, protons and heavy ions; the heavy ions, in laboratory plasmas, may be as impurities and in some natural plasmas as a genuine constituent, e.g., solar wind is composed of electrons, protons and α-particles (helium) and cometary plasmas have water group ions. To study the chaotic processes in such multispecies plasmas, starting from the corresponding multi fluid equations we derived the evolution equation[16,31], which is given by:

$$\frac{\partial B}{\partial t} + \alpha \frac{\partial}{\partial x}\left(B \mid B \mid^2\right) \pm i\mu \frac{\partial^2 B}{\partial x^2} = 0. \tag{28}$$

with α and μ defined by:

$$\alpha = \frac{1}{4} \sum_s \frac{\rho_{so}^2 \left(1 - Z_s \delta\right)}{\left(\rho_{so} - \gamma_s P_s\right)}, \tag{29a}$$

$$\mu = \frac{1}{2} \sum_s \frac{\rho_{so}}{Z_s}, \tag{29b}$$

$$\delta = \sum_s \frac{\rho_{so} Z_s \gamma_s P_s}{\left(\rho_{so} - \gamma_s P_s\right)} \left[\sum_s \frac{Z_s^2 \rho_{so}^2}{\left(\rho_{so} - \gamma_s P_s\right)}\right]^{-1}, \tag{29c}$$

where subscript s refers to different species, γ is the ratio of the specific heat and Z is the charge to mass ratio. As a result of this, the localized stationary Alfvén waves that are driven by a harmonic driver can be represented by the following set of equations:

$$\frac{dB_y}{d\xi} = \frac{\partial H}{\partial B_z} + \frac{A}{2\,\mu} \cos\theta, \tag{30a}$$

$$\frac{dB_z}{d\xi} = -\frac{\partial H}{\partial B_y} + \frac{A}{2\,\mu} \sin\theta, \tag{30b}$$

$$\frac{\partial \theta}{\partial \xi} = \Omega, \tag{30c}$$

where A is the amplitude of the driver and H is the Hamiltonian given by,

$$H\left(\vec{B}\right) = \frac{1}{2}\alpha\left(1 - \beta\right)\left(B^2 - 1\right)^2 - \frac{\Lambda}{2}\left(\vec{B} - \hat{e}_y\right)^2, \tag{31}$$

with $\xi = (x - Vt)/\mu$ and

$$\Lambda = \frac{2(1-\beta)}{\mu}\left(\frac{V}{b_0^2} - \alpha\right) \tag{32}$$

To see the effect of the heavier species, here we will present the results of cometary plasma with oxygen ions as the third species and also for the dusty plasmas.

A. Cometary Plasma

For cometary plasma with 10% oxygen in abundance, Poincare maps, for the two-species and the three-species plasmas, are shown in Figs.10 and 11 respectively[31,44–46]. For both the figures, the driver is the left hand driver. Since all the parameters for both the figures are the same, Fig.11 shows the effect of the heavy ions (oxygen). Fig.10 shows that even for a weak driver corresponding to $A = 0.3$, or even for smaller A (not shown here), Alfvén waves in a 2 - species plasma (without any heavy ions or dust grains) become chaotic. However, as shown in Fig.11, in the presence of the heavier oxygen ions, the chaos appears only when the driver is relatively much stronger. From comparison of these two figures, it is evident

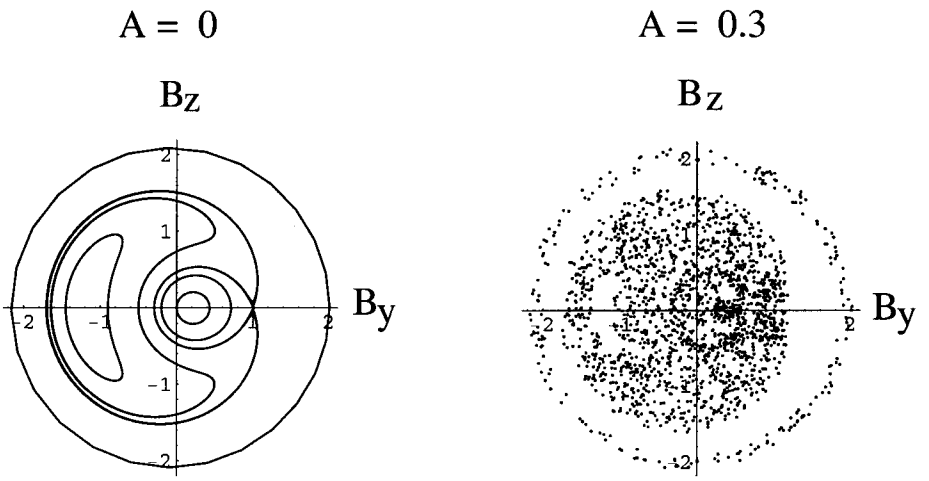

FIG. 10. Poincaré maps for a driven Alfvénic system in a 2-species plasma.

that the chaos is reduced due to the presence of the oxygen - in other words, the threshold for chaos goes up because of heavy ions. Physically this could be interpreted as the inertial

stabilization due to the heavy ions.

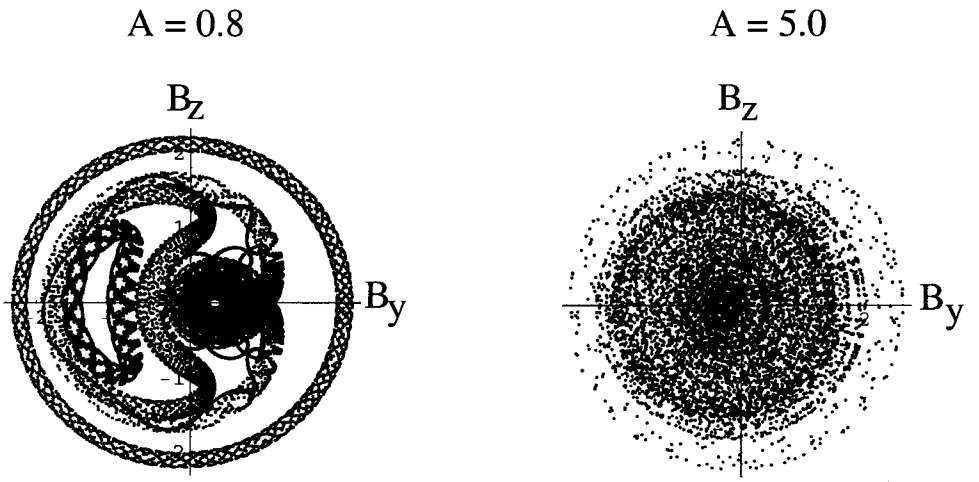

FIG. 11. Poincaré maps for a driven Alfvénic system in 3-species cometary plasma with water group ions.

B. Dusty Plasmas

Dusty plasmas are prevalent in many cosmic as well as space plasmas such as planetary rings, planetary magnetospheres, cometary environment, interstellar medium etc.[47–50]. Here we would like to distinguish between plasmas with a few dust grains and the plasmas where dust grains, satisfying the condition $N_d\ \lambda_d^3 >> 1$ (N_d being the density of charged dust grains and λ_d the Debye length), form the third constituent of the plasma. Only the latter ones we would define as dusty plasmas; such plasmas, one encounters in process plasma e.g., chip manufacture besides the cosmic plasmas. Unlike the ordinary plasmas, dusty plasmas have very massive heavily charged dust grains. Moreover the charge fluctuations in dusty plasmas can be very significant. Nonlinear Alfvén waves in dusty plasmas are governed by[51],

$$\frac{\partial \vec{B}_\perp}{\partial t} + \alpha_1 \frac{\partial}{\partial x}\left(\vec{B}_\perp \mid \vec{B}_\perp \mid^2\right) + \mu_1 \left(\hat{e}_x \times \frac{\partial^2 \vec{B}_\perp}{\partial x^2}\right) + \delta_1 \vec{B}_\perp = 0. \tag{33}$$

Eq. (33) is same as the one for multispecies plasmas[16,31] except for the additional (last term) source term which is due to charge fluctuations of the dust grains. The co-efficients α_1, μ_1 and δ_1 for cold plasmas are given by:

$$\alpha_1 = \frac{1}{4\,g}, \tag{34a}$$

$$g = \sum_s \rho_s\,(V - U_s)\,, \tag{34b}$$

$$\mu_1 = \frac{1}{2g} \sum_s \frac{\rho_s\,(V - U_s)^3}{\Omega_s}, \tag{34c}$$

$$\delta_1 = \frac{1}{2g} \sum_s \sum_r \left(\rho_s\,\gamma_{sr} - \rho_r\,\gamma_{rs}\right) U_r, \tag{34d}$$

where ρ_s is the mass density , Ω_s is the cyclotron frequency and U is the drift velocity in equilibrium. Note that in the absence of any equilibrium drift i.e., for $U_s = 0$, the source term vanishes; in this case V reduces to the Alfvén speed ($V_A = (B_o/(4\pi\,\rho)^{1/2})$. For 3-species plasma with electrons, protons and heavy dust grains, these coefficients are simply given by,

$$\alpha_1 = \frac{1}{4}\left(1 + \frac{\rho_d}{(\rho_e + \rho_p)}\right)^{-1/2}, \tag{35a}$$

$$\mu_1 = \frac{1}{2g}\left(1 + \frac{\rho_d}{(\rho_e + \rho_p)}\right)^{-2}\left(1 + \frac{\rho_d\,\Omega_p}{\rho_p\,\Omega_d} + \frac{\rho_e\,\Omega_p}{\rho_p\,\Omega_e}\right), \tag{35b}$$

$$\delta_1 = 0. \tag{35c}$$

In Eqs.(35), the subscripts e, p and d represent electrons, protons and dust grains respectively. For 2-species plasma i.e., for $N_d = 0$, note that $V = g = 1$, $\alpha_1 = 1/4$ and $\mu_1 = 1/2$. In writing Eqs.(34), we have made use of the charge neutrality condition, i.e., $(N_e + Z_d N_d) = N_p$. In the presence of an external driver, Eq. (33) gets modified; the source term $S(\vec{B}_\perp, x, t)$ appears on the right hand side of Eq. (33)[39]. For a plane circularly polarized driver i.e., for S = A exp (i k ξ), Eq. (33) can be written in terms of the Hamiltonian of the system[31,46], namely

$$\frac{dB_y}{d\xi} = -\frac{\partial H}{\partial B_z} - \frac{A}{2\,\mu_1}\cos\theta, \tag{36a}$$

$$\frac{dB_z}{d\xi} = \frac{\partial H}{\partial B_y} - \frac{A}{2\,\mu_1}\,\sin\theta, \tag{36b}$$

$$\frac{\partial \theta}{\partial \xi} = \Omega, \tag{36c}$$

where $\xi = (x - V\,t)\,/\,2$, A and Ω as the amplitude and the frequency of the driver and H the Hamiltonian that is given by,

$$H\left(\vec{B}\right) = \frac{1}{2}\,\frac{\alpha_1}{\mu_1}\,\left(B^2 - 1\right)^2 - \frac{\Lambda_1}{2}\,\left(\vec{B} - \hat{e}_y\right)^2, \tag{37}$$

with

$$\Lambda_1 = \frac{2}{\mu_1}\,(\frac{V}{b_0^2} - \alpha_1) \tag{38}$$

and b_0 as the asymptotic value of B.

As mentioned earlier, dusty plasmas are observed in nebulas, planetary rings, planetary magnetospheres and cometary environment. We have solved Eq. (36) numerically for the case of rings of Saturn and for the cometary cases. In these systems, dust grain size is typically a few microns and dust mass is of the order of $10^{12}\ m_p$. The dust grains carry very high charges[50] ; typically $Z_d \sim (10^3 - 10^4)e$. However the dust number densities could be as low as $(10^{-8} - 10^{-6})\ N_p$. For these parameters α_1 and μ_1 simply reduce to,

$$\alpha_1 \simeq \frac{1}{4}\,(\frac{\rho_p}{\rho_d})^{1/2} \tag{39}$$

and

$$\mu_1 \simeq \frac{1}{2}\,\frac{\rho_p\,\Omega_p}{\rho_d\,\Omega_d} = \frac{1}{2}\,\frac{N_p}{N_d\,Z_d}. \tag{40}$$

Thus it is apparent that the crucial parameters, governing the nonlinear dynamics, are the mass density and the charge of the dust grains.

The results of numerical computations are shown in Figs.12 and 13. Fig.10 shows that even for a weak driver corresponding to $A = 0.3$, Alfvén waves in a 2 - species plasma (without the dust grains) become chaotic. However in dusty plasmas as shown in Fig.12 for

cometary plasmas and in Fig.13 for Saturn rings, Poincare maps do not show any chaos. One gets only periodic orbits even for strong drivers with amplitudes which are order of magnitude larger compared to the one for 2 - species plasma. From these results (Figs.12 and 13), we can straightaway conclude that the chaos in Alfvénic systems simply disappears due to the presence of massive dust grains.

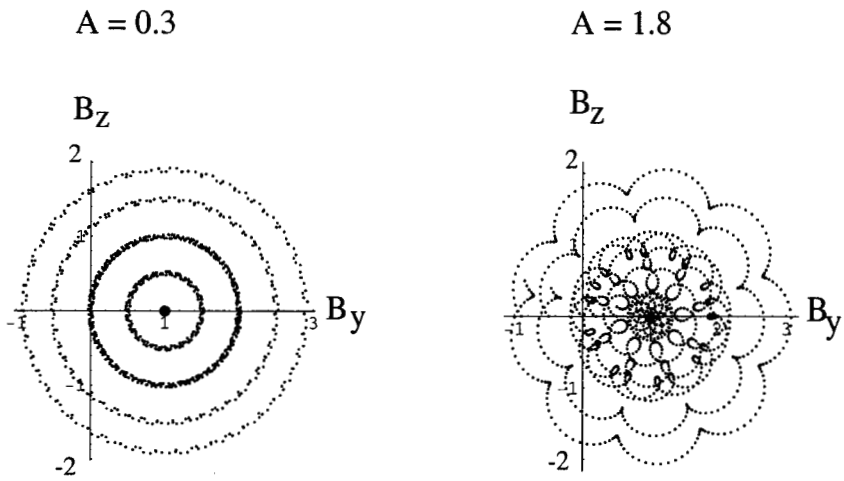

FIG. 12. Same as Fig.10 but with the dust grains with $N_d/N_p = 1.7 \times 10^{-4}$, $Z_d = 10^3$, $m_d \,/\, m_p = 10^{12}$.

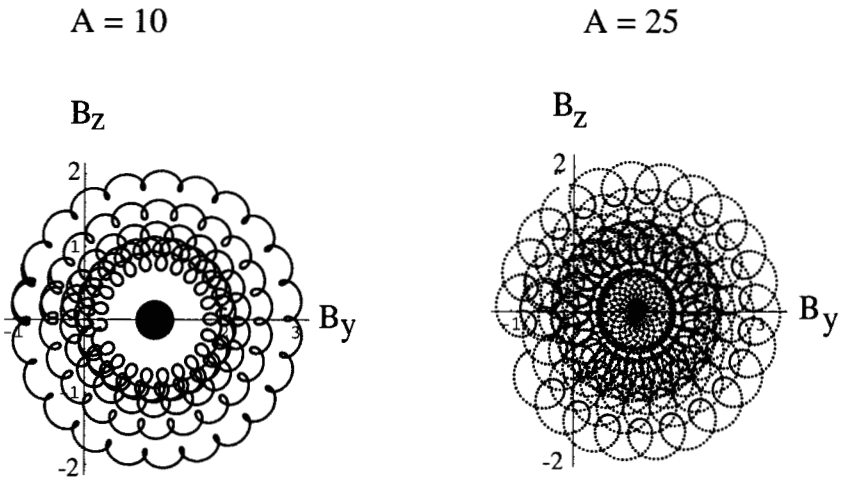

FIG. 13. Same as Fig.12 but for Saturn Rings with $N_d/N_p = 4 \times 10^{-8}$, $Z_d = 10^4$.

Here we have confined ourselves to dusty plasmas but this technique can be fruitfully used for controlling chaos in other plasmas e.g., fusion plasmas also. All that one has to do

is to introduce a small fraction of heavy ions, like an impurity, in the region that is chaotic.

V. MHD SIMULATIONS

As mentioned above, for large amplitude waves ($\delta B/B \geq 1$), the approximations made in the derivation of the DNLS / MDNLS equations become invalid because the derivation includes terms only up to cubic nonlinearities. Moreover these evolution equations are not valid for $\beta \sim 1$. For $\beta \sim 1$, coupling between Alfvén waves and ion acoustic waves becomes

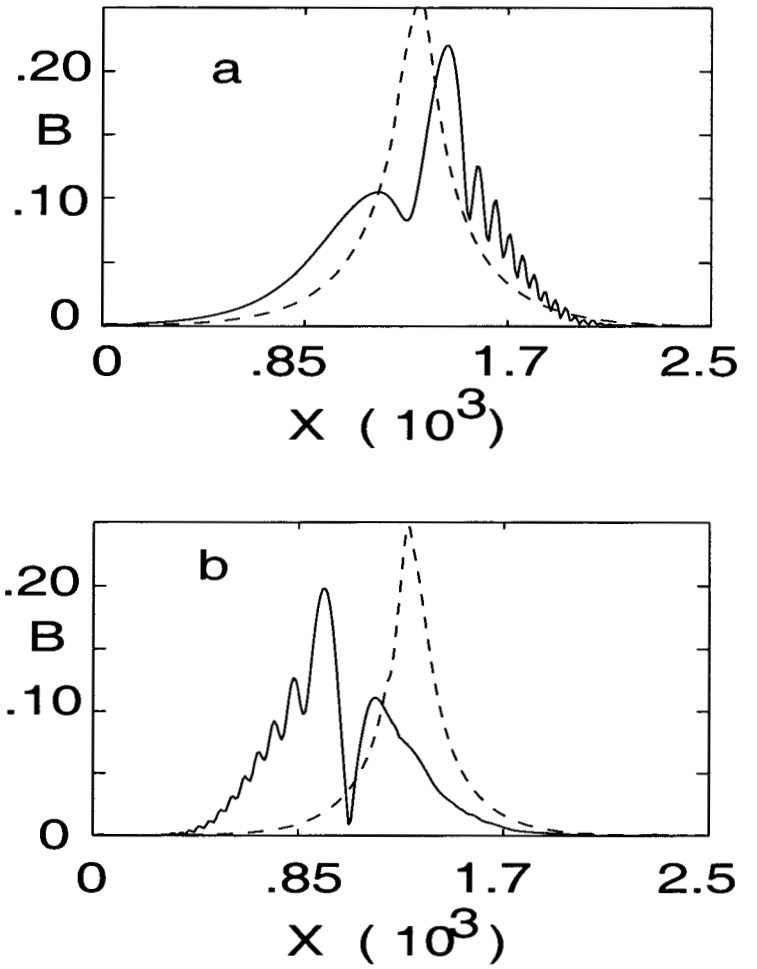

FIG. 14. Evolution of magnetic field fluctuations for a RHP soliton for a) $\beta = 0.3$, and b) $\beta = 1.5$ at $t = 0$ (dashed line) and $t = 5000$ (solid line)

significant. one could overcome these limitations by doing simulations. For this purpose let

us go back to the full set of Hall-MHD equations, namely Eqs. (2) - (6). These equations are solved by using periodic boundary conditions and by taking the DNLS soliton solution,

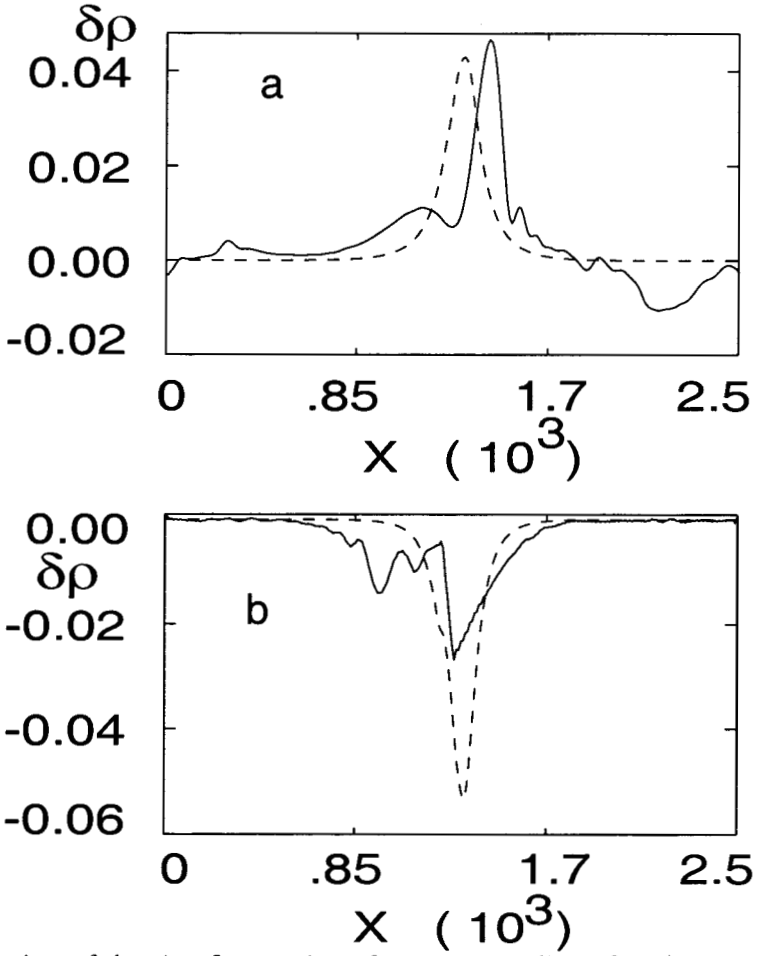

FIG. 15. Evolution of density fluctuations for a RHP soliton for a) $\beta = 0.3$, and b) $\beta = 1.5$ at $t = 0$ (dashed line) and $t = 5000$ (solid line)

given by Eqs. (25) - (27), as an initial condition[21,22]. Unlike fusion plasmas, some of the space plasmas have $\beta > 1$. In the solar wind, β, T_e and T_i all vary with heliospheric distance. In particular, β spans the entire range from $\beta < 1$ to $\beta > 1$. To investigate the stability of the initial DNLS soliton, we have done the simulations for different values of β; spatio - temporal evolutions of the RHP solitons are shown in Figs. 14 and 15. We observe a wave train on the leading edge for $\beta < 1$ (cf. Fig.14a) and on the trailing edge for $\beta > 1$ (cf. Fig.14b). However in both cases the amplitude of the soliton goes down. It is interesting to compare this with the evolution of the magnetic field of the LHP initial soliton. In the latter

case wave train appears on the leading edges[21] for $\beta < 1$ as well as for $\beta > 1$. Moreover, in this case the amplitude was found to increase (decrease) for $\beta < 1 (> 1)$ as the soliton evolved. We had observed similar behaviour [22] for plasmas with much smaller β e.g., solar corona with $\beta = 0.05$. Buti et al.[21] had considered the case with much higher β also and showed that for $\beta = 3$ for the RHP soliton, by $t = 5000$, the wave train disappears. So it is pretty obvious that the soliton is disrupted simply because of the higher order nonlinearities that are neglected in the DNLS / MDNLS equations. In fact we had shown[22] that the disruption time scales as B_s^{-4}. The density fluctuations that are taken as sort of static in the DNLS description, are also found to evolve (see Fig.15). Unlike the driven soliton that evolves into fully developed turbulence (see Fig.9) through chaotic channels, in all the cases that we have considered so far[21,22] for our MHD simulations, we find that neither the higher order nonlinearities nor the coupling of magnetic field and density fluctuations lead to Alfvénic turbulence. We are persuing the MHD as well as hybrid simulations with larger-amplitude solitons to see if there is any possibility of generating turbulence through nonchaotic channels.

VI. CONCLUSIONS

The coherent properties of the DNLS solitos are destroyed by a variety of sources, e.g., inhomogeneities in the plasma densities and the magnetic fields, coupling of magnetic field and density fluctuations, higher order nonlinearities that are neglected in the derivation of the evolution equation and some external source like a harmonic driver. The right-hand polarized soliton is much more robust compared to the left-hand polarized one. However both, under different conditions can lead to chaotic Alfvén waves and the chaos in turn leads to Alfvénic turbulence. The power spectra of the magnetic field is found to be very similar to the one observed in the solar wind. The phenomena of self-organization and collapse are also observed during the dynamical evolution of the Alfvén waves.

VII. ACKNOWLEDGEMENTS

The research conducted at the Jet Propulsion Laboratory, California Institute of Technology, was performed under contract to the National Aeronautics and Space Administration. I would like to the acknowledge the financial support from the National Research Council. I would also like to express my gratitude to all my co-authors of all the cotributions used for the present review.

---

[1] M. Pettini, L. Nocera, and A. Vulpiani, in *Chaos in Astrophysics, eds. J.R. Buchler et al., Dordrecht: Reidel*, **305** (1985).

[2] G.S. Lakhina and B. Buti, *Solar Phys.*, **99,** 277 (1985); *Astrophys. J.*, **327**, 1020 (1988); *Astrophys. J.*, **352**, 747 (1990).

[3] S.R. Spangler,*Astrophys.J.*, **376**, 540 (1991).

[4] V. Jatenco-Pereira, *Physica Scripta*, **T60**,113 (1995).

[5] J. W. Belcher and L. Davis, *J. Geophys. Res.*, **76,** 3534 (1971).

[6] F. L. Scarf, et al., *Science*, **232**, 377 (1986).

[7] L.F. Burlaga, *Rev. Geophys. Space Phys.*, **21**, 363 (1983).

[8] E. Marsch and S. Liu, *Ann. Geophys.*, **11**, 227 (1993).

[9] C.-Y. Tu and E. Marsch, *Space Sci. Rev.*, **73**, 1 (1995).

[10] Macek, W.M., Testing for an Attractor in the Low-Speed Solar Wind Flow in *Solar Wind Nine*, Eds. S. Habbal et al., American Institute of Physics, (1999).

[11] D.J. Kaup and A.C. Newell, *J. Math. Phys.* **19**. 798 (1978).

[12] C. F. Kennel, B. Buti, T. Hada and R. Pellat, *Phys. Fluids*, **31**, 1949 (1988).

[13] B. Buti, Nonlinear and Chaotic Alfvén waves, in *Solar and Planetary Plasma Physics,* Ed. B. Buti, p 92, World Scientific, Singapore (1990).

[14] A. Rogister, *Phys. Fluids* **14**, 2733 (1971).

[15] T. Hada, C.F. Kennel and B. Buti, *J. Geophys. Res.*, **94**, 65 (1989).

[16] F. Verheest and B. Buti, *J. Plasma Phys.*, **47**, 15 (1992).

[17] E. Mjolhus and J. Wyller, *Physica Scripta,***33**, 442 (1986); *Jou. Plasma Phys.*, **40**, 299 (1988).

[18] S.R. Spangler, *Phys. Fluids,* **B1**, 1738 (1989); *Phys. Fluids,* **B2**, 407 (1990).

[19] M.V. Medvedev and P.H. Diamond, *Phys. Plasmas,* **3**, 863 (1996).

[20] T. Hada, *Geophys. Res. Lett.,***20,** 2415 (1993).

[21] B. Buti, V.Jayanti, A.F. Viñas, S. Ghosh, M.L. Goldstein, D.A. Roberts, G.S. Lakhina and B.T. Tsurutani, *Geophys. Res. Letts.,* **25**, 2377 (1998).

[22] M. Velli, B. Buti, B.E. Goldstein and R. Grappin, Propagation and Disruption of Alfvénic solitons in the Expanding Solar Wind in *Solar Wind Nine*, Eds. S. Habbal et al., American Institute of Physics (1999).

[23] B. Buti, P.C. Liewer, B.E. Goldstein and M. Velli, to be submitted (1999).

[24] N. Nocera and B. Buti, Low Dimensional Structures in Numerical Simulations of DNLSE, *Proc. 94ICPP,* Eds P.H. Sakanaka, E. Del Bosco and N.V. Alves, p 115 ,INPE, Sao Jose dos Campos, SP, Brazil (1995).

[25] N. Nocera and B. Buti, *Physica Scripta, T63*, 186 (1996).

[26] N. Nocera and B. Buti, Bifurcations of Coherent States of the DNLS Equation, in *New Perspectives in the Physics of Mesoscopic Systems,* Eds S. De Martino et al., p 225, World Scientific, Singapore (1997).

[27] N. Nocera and B. Buti, *Cont. Fusion and Plasma Phys.,* **22C**, 2295 (1998).

[28] B. Buti and L. Nocera, Chaotic Alfvén Waves in the Solar Wind in *Solar Wind Nine*, Eds. S. Habbal et al., American Institute of Physics (1999).

[29] A. Roychoudhury, B. Buti and B. Dasgupta , *Australian J. Phys.*, **51**, 125 (1997).

[30] T. Tanuiti and C. C. Wei, *J. Phys. Soc. Japan,* **24**, 941 (1968).

[31] B. Buti, *J. Geophys. Res.,* **97** , 4229 (1992).

[32] B. Buti, . *Phys. Lett. A,* **235**, 241 (1997).

[33] B. Buti, *Geophys. Res. Lett.*, **18**, 809 (1991).

[34] B. Buti, V.L. Galinski, V.I. Shevchenko, G.S. Lakhina, B.T. Tsurutani, B.E. Goldstein, P. Diamond and M.V. Medvedev, *Astrophys. J.*, in press (1999).

[35] C. Canuto, M.Y. Hussaini, A. Quarteroni and T.A. Zang, *Spectral Methods in Fluid Dynamics* (Springer Verlag, New York), p 84 (1987).

[36] E. Mjolhus, *J. Plasma Phys.,* **19**, 437 (1978).

[37] M. Mohan and B. Buti, *Plasma Phys.,* **21**, 713 (1979).

[38] B. Bavassano, M. Dobrowolny, F. Mariani and N.F. Ness, *J. Geophys. Res.,* **87**, 3617 (1982).

[39] T. Hada, C. F. Kennel, B. Buti and E. Mjolhus, *Phys. Fluids,* **B2**, 2581 (1990).

[40] B. Buti and L. Nocera, *Phys. Plasmas*, submitted (1999).

[41] V.E. Zakharov, Collapse and Self-Focusing of Langmuir Waves, in *Handbook of Plasma Physics,* Eds M.N. Rosenbluth and R.Z. Sagdeev, p 81, Elsevier Science Publisher (1984).

[42] B. Buti, Evolution and Control of Chaos in Plasmas, in *Nonlinear Dynamics and Computational Physics*, Ed. V.B. Sheorey, p 177, Narosa publisher, London (1998).

[43] E. Ott, C. Grebogi and J.A. York, *Phys. Rev. Lett.* **64**, 1196 (1990).

[44] B. Buti, *Astrophys. Spaca Sci.,* **243**, 33 (1996).

[45] B. Buti, *PRAMANA (Jou. of Phys.)*, **49**, 93 (1997).

[46] B. Buti, *Phys. Lett. A*, **235**, 241 (1997).

[47] L. Spitzer Jr., *Physical Processes in Interstellar Medium, Wiley, New York* (1978).

[48] C.K. Goertz, *Rev. Geophys.* **27**, 271 (1989).

[49] T.G. Northrop, *Physica Scripta*, **45**, 475 (1992).

[50] D.A. Mendis and M. Rosenberg, *Ann Rev. Astron. Astrophys.* **32**, 419 (1994).

[51] F. Verheest and P. Meuris, *Phys. Lett.* **210A**,198 (1996).